



Discovery of $^{14}\text{NH}_3$ (2,2) Maser Emission in Sgr B2 Main

E. A. C. Mills¹, A. Ginsburg², A. R. Clements^{3,10}, P. Schilke⁴, Á. Sánchez-Monge⁴,
K. M. Menten⁵, N. Butterfield⁶, C. Goddi⁷, A. Schmiedeke⁸, and C. G. De Pree⁹

¹ Physics Department, Brandeis University, 415 South Street, Waltham, MA 02453, USA; elisabeth.ac.mills@gmail.com

² National Radio Astronomy Observatory, ¹¹ 1003 Lopezville Road, Socorro, NM 87801, USA

³ Department of Chemistry, University of Virginia, Charlottesville, VA 22904, USA

⁴ I. Physikalisches Institut, Universität zu Köln, Zùlpicher Str. 77, D-50937 Köln, Germany

⁵ Max-Planck-Institut für Radioastronomie, Auf dem Hügel 69, D-53121 Bonn, Germany

⁶ Green Bank Observatory, 155 Observatory Road, PO Box 2, Green Bank, WV 24944, USA

⁷ Department of Astrophysics/IMAPP, Radboud University, PO Box 9010, 6500 GL Nijmegen, The Netherlands

⁸ Max Planck Institute for Extraterrestrial Physics, Giessenbachstrasse 1, D-85748 Garching, Germany

⁹ Department of Physics & Astronomy, Agnes Scott College, 141 East College Avenue, Decatur, GA 30030, USA

Received 2018 October 22; revised 2018 November 15; accepted 2018 November 19; published 2018 December 10

Abstract

We report the discovery of the first $^{14}\text{NH}_3$ (2,2) maser, seen in the Sgr B2 Main star-forming region near the center of the Milky Way, using data from the Very Large Array radio telescope. The maser is seen in both lower-resolution ($3''$ or ~ 0.1 pc) data from 2012 and higher-resolution ($0''.1$ or ~ 1000 au) data from 2018. In the higher-resolution data NH_3 (2,2) maser emission is detected toward five independent spots. The maser spots are not spatially or kinematically coincident with any other masers in this region, or with the peaks of the radio continuum emission from the numerous ultracompact and hypercompact H II regions in this area. While the (2,2) maser spots are spatially unresolved in our highest-resolution observations, they have unusually broad line widths of several kilometers per second, which suggests that each of these spots consists of multiple masers tracing unresolved velocity structure. No other NH_3 lines observed in Sgr B2 Main are seen to be masers, which continues to challenge existing models of NH_3 maser emission.

Key words: ISM: molecules – masers – stars: formation

1. Introduction

Ammonia masers are relatively rare, and have been seen in only a handful of sources, mainly high-mass star-forming regions. Despite this rarity, many different $^{14}\text{NH}_3$ (J, K) inversion transitions, both nonmetastable ($J \neq K$) and metastable ($J = K$), have been observed to be masers (e.g., Wilson & Schilke 1993). Maser action has even been reported to occur in a transition of the rare isotopologue $^{15}\text{NH}_3$ (Mauersberger et al. 1986; Johnston et al. 1989; Gaume et al. 1991; Schilke et al. 1991).

$^{14}\text{NH}_3$ masers arising from nonmetastable energy levels are seen more frequently than metastable masers. This is likely due to the smaller population of these levels, which quickly decay unless excited by extreme densities or intense radiation fields, and are thus easier to invert (Wilson & Schilke 1993). The most common of these appear to be in the ortho- NH_3 ($K = 3n$) transitions (9,6) and (6,3) (Madden et al. 1986; Pratap et al. 1991; Wilson & Schilke 1993). However, few surveys for nonmetastable $^{14}\text{NH}_3$ masers are reported in the literature (Madden et al. 1986 report surveying 17 regions for maser emission, but only finding masers in 4 of these), and ultimately these masers have only been reported toward five regions: W51, W49, DR21, NGC 7538, and NGC 6334. Additional masing nonmetastable transitions, including para- NH_3 transitions, have been observed in W51 (Mauersberger et al. 1987; Wilson & Henkel 1988; Wilson et al. 1990; Henkel et al. 2013), NGC 7538 (Hoffman & Kim 2011; Hoffman & Joyce 2014), and NGC 6334 (Walsh et al. 2007).

Of the metastable $^{14}\text{NH}_3$ masers, the most commonly observed masing transition is the ortho (3,3) line, which has been definitively seen toward DR21(OH), W51 North, and G5.89-0.39 (Mangum & Wootten 1994; Zhang & Ho 1995; Hunter et al. 2008), and which has been suggested to also be a maser in a variety of other sources, including NGC 6334, the southern part of Sgr B2, and the nucleus of the starburst galaxy NGC 253 (Kraemer & Jackson 1995; Martin-Pintado et al. 1999; Ott et al. 2005). Other ortho lines—(6,6), (9,9), and (12,12)—have also been reported to exhibit maser action in NGC 6334 (Walsh et al. 2007) and W51 (Henkel et al. 2013; Goddi et al. 2015). Para- NH_3 masers are rarer; however, masers have been reported in the (1,1) line toward the DR21 H II region (Gaume et al. 1996), in the (5,5) line toward G9.62 +0.19 (Hofner et al. 1994) and in the (7,7) line toward W51 North (Goddi et al. 2015).

We report the discovery of a new, strong para- $^{14}\text{NH}_3$ maser in the metastable (2,2) transition toward the Galactic center star-forming region Sgr B2 Main (hereafter Sgr B2 (M)). Sgr B2 is the most massive molecular cloud in the central 500 pc of the Galaxy, accounting for 10% of the mass in this region (Scoville et al. 1975). This cloud hosts the most intense ongoing star formation in the Galactic center, much of which is concentrated in two sites of clustered star formation: Sgr B2 (M) and Sgr B2 North (N). Sgr B2 (M) is thought to be older than Sgr B2 (N), as it is less chemically rich (Corby et al. 2015; Sánchez-Monge et al. 2017) and appears to be more fragmented (Qin et al. 2011; Sánchez-Monge et al. 2017; Ginsburg et al. 2018). In addition to containing a fragmented, massive hot core (Vogel et al. 1987; Qin et al. 2011; Sánchez-Monge et al. 2017), it contains dozens of ultracompact and hypercompact H II regions (De Pree et al. 1998). Sgr B2 (M) also contains at least one molecular outflow

¹⁰ A. Ginsburg is a Jansky Fellow of the National Radio Astronomy Observatory.

¹¹ The National Radio Astronomy Observatory is a facility of the National Science Foundation operated under cooperative agreement by Associated Universities, Inc.

traced by H₂O masers, ¹⁴NH₃ emission and absorption, and millimeter H₂CO lines (Vogel et al. 1987; McGrath et al. 2004; Qin et al. 2008). In this Letter, we present new high-resolution centimeter-wave observations of ¹⁴NH₃ toward this region, and discuss the detected (2,2) maser emission both in the context of other star formation indicators detected in this specific region, and in the context of NH₃ masers in general.

2. Data

2.1. Low-resolution Observations

Observations of ¹⁴NH₃ toward Sgr B2 (M) were made using the Karl G. Jansky Very Large Array (VLA), a facility of the National Radio Astronomy Observatory in January 2012 in DnC configuration using the *K*-band receivers (project 11B-210, PI: E.A.C. Mills). For the ¹⁴NH₃ (2,2) line at 23.7226333 GHz, the synthesized beam size was 2''.83 × 2''.56, which corresponds to a spatial resolution of 0.1 pc at the adopted distance to Sgr B2 of 8 kpc (Reid et al. 2009; Gravity Collaboration et al. 2018). The velocity resolution of the (2,2) line observations was 1.58 km s⁻¹. In addition to the (2,2) line, the (1,1) through (7,7) and (9,9) metastable ¹⁴NH₃ lines were also observed, along with the (10,9) nonmetastable line. The observations toward the Sgr B2 cloud were part of a larger survey of Galactic center clouds; additional description of these observations, including details on the data calibration and imaging, is given in Mills et al. (2015).

2.2. High-resolution Observations

Observations of ¹⁴NH₃ toward Sgr B2 (M) were also made using the A configuration of the VLA in 2018 March–April (project 18A-229, PI: A. Ginsburg). These observations had a spatial resolution of 0''.17 × 0''.08 (1360 × 640 au) and a velocity resolution of 0.79 km s⁻¹ for the (2,2) line. Other observed lines of ¹⁴NH₃ included (1,1), (2,2), (4,4), (5,5), (7,7), (2,1), (3,2), (5,3), and (5,4), however the (3,2) line was not observed in all sources as it was on the edge of a sub-band, which limited the frequency coverage.

The data were pipeline processed using the VLA pipeline after removing the automated RFI flagging step. We then performed three iterations of phase-only self-calibration using the brightest ¹⁴NH₃ (2,2) maser peak.

2.3. Absolute Positional Reference Frame

We define the absolute positional reference frame for these observations using a high-resolution (0''.2), 3 mm Atacama Large Millimeter/submillimeter Array (ALMA) continuum map (Project code 2016.1.00550.S, PI: A. Ginsburg), which should have good absolute positional accuracy as it is tied to a larger mosaic of the region (Ginsburg et al. 2018). We use the task “register_translation” from the python package scikit-image (van der Walt et al. 2014) to perform cross correlations between the ALMA image and our A-configuration continuum image, and shift our A-configuration images by 0''.05 in R.A. and 0''.48 in decl. The uncertainty in the alignment from the cross correlation is ±0''.03. This large offset is due to an error in the VLA calibrator catalog for the position of source J1744-3116, which is used as a phase calibrator for the A-configuration data (L. Sjouwerman 2018, private communication).

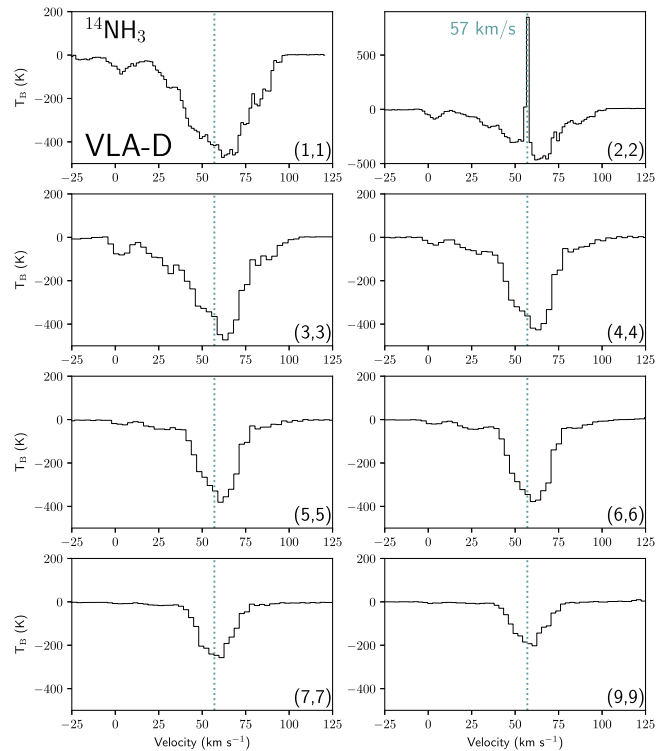


Figure 1. Spectra of ¹⁴NH₃ metastable transitions from VLA DnC-configuration observations. All transitions are seen in absorption against the “F” complex of H II regions in Sgr B2 (M) except the (2,2) line, where maser emission is also seen at a velocity of 57 km s⁻¹. This velocity is indicated by a vertical dotted line in each panel.

3. Results

Of the 13 observed transitions of ¹⁴NH₃ (10 of which were observed in A configuration), we only detect maser emission in the (2,2) line¹². The A-configuration observations of ¹⁴NH₃ (5, 4) also overlap with the ¹⁵NH₃ (2,2) line, which we can confirm does not show similar maser emission. In Figure 1 we show spectra from the DnC-configuration observations in which we see a single, narrow (the line is unresolved for a channel width of 1.5 km s⁻¹) maser component at 57 km s⁻¹, in the midst of broad absorption that is seen in all of the observed ¹⁴NH₃ lines. In the A configuration, this maser breaks up into five independent spots spread out over 2'' at velocities from 57 to 69 km s⁻¹, with measured velocity widths of 1.6–3.9 km s⁻¹. We show spectra of all the ¹⁴NH₃ lines toward the brightest maser spot in Figure 2, and profiles of the (2,2) line toward each of the five detected maser spots in Figure 3. The (2,2) maser appears to be a persistent feature over a large time baseline, as it is not only seen in our 2012 and 2018 observations, but can be seen in Figure 6 of Vogel et al. (1987), where there is a negative optical depth (i.e., emission) at a velocity of ~60 km s⁻¹.

¹² We investigate other possible line identifications for this maser, and find that there only three species that have been detected toward Sgr B2 (M) that have transitions lying within ~10 km s⁻¹ of the (2,2) line: HCOOCH₃ (and its isotopologue H¹³COOCH₃, which has not been detected but is likely present), ¹⁷OH and CH₃OCH₃. However, none of these are a plausible candidate for this maser, as these species have either never been observed to be masers in the interstellar medium (ISM; ¹⁷OH and CH₃OCH₃) or have only been observed to be weak masers with widths similar to those of thermally excited lines (Faure et al. 2014), which is inconsistent with the narrower profiles seen in our observations.

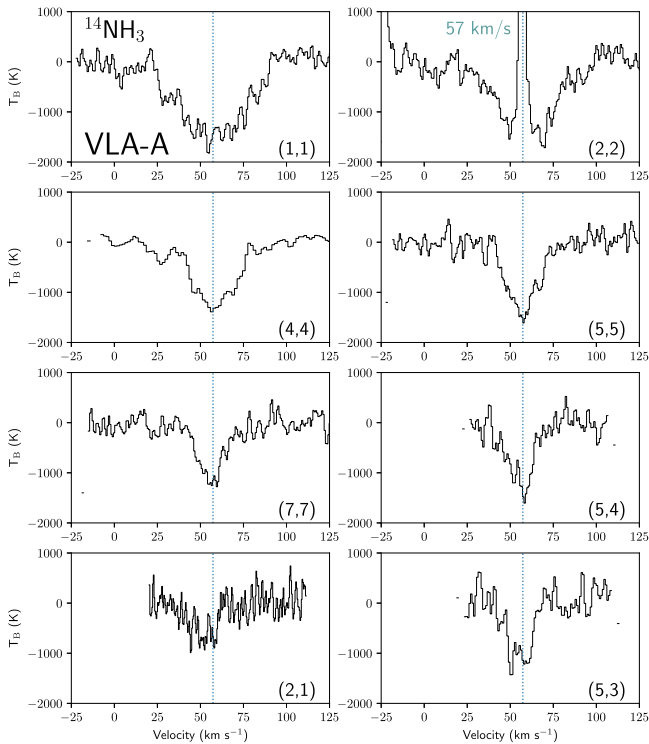


Figure 2. Spectra of $^{14}\text{NH}_3$ metastable and nonmetastable transitions from the VLA A-configuration observations toward the position of Maser M1, the strongest (2,2) maser spot. All transitions are seen in absorption against the “F” complex of H II regions in Sgr B2 (M) except the (2,2) line, where the maser emission is seen at a central velocity of $\sim 57 \text{ km s}^{-1}$ (vertical dotted line). The y-axis of all of the plots has been scaled to the same range to emphasize the absorption present in all transitions; the peak of the (2,2) maser emission is $9 \times 10^4 \text{ K}$.

The positions of the $^{14}\text{NH}_3$ masers are shown in Figure 4. The brightest maser is M1, which has a peak intensity of 0.5 Jy, or a brightness temperature of $T_B > 9 \times 10^4 \text{ K}$.¹³ M2 is only slightly offset from M1, and its spectrum contains an additional emission contribution from the sidelobes of M1; it may peak nearer to a velocity of 59 km s^{-1} with $T_B > 7000 \text{ K}$. M3 is offset by $\sim 1''$ from M1 and has $T_B > 3900 \text{ K}$. M4 and M5 are much weaker, having limits on T_B of only $>700 \text{ K}$. While this could be considered consistent with thermal emission, as temperatures $>1000 \text{ K}$ have been measured toward Sgr B2 (M) (Wilson et al. 2006), no correspondingly bright emission is seen in the other NH_3 lines, indicating that these sources are also nonthermal. Maser spots M1–M4 are on the edge of continuum sources, and the maser emission toward these regions is superimposed on a broad absorption feature. However, M5 is not near to any known continuum source, and shows a weak thermal emission rather than absorption profile in the other NH_3 lines. In Table 1 we list the properties of each detected maser spot, including its position, central velocity, velocity width, and peak brightness temperature.

Based on the correspondence between the absorption and emission seen in the A-configuration observations, we believe it is most likely that the main hyperfine component¹⁴ of the (2,2) line is masing (while this is assumed for most observed

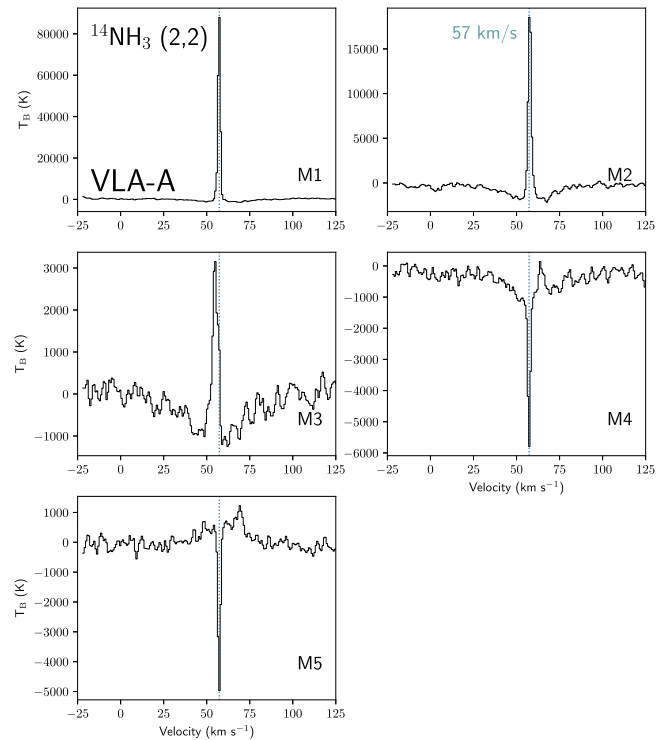


Figure 3. Spectra of the $^{14}\text{NH}_3$ (2,2) line toward each of the maser spots seen in the A-configuration data. Maser spots M1–4 are superimposed on absorption against nearby H II regions, while M5 lies on top of a broad, thermal emission profile. The central velocity of M1, the brightest maser source, is shown as a vertical dotted line at 57 km s^{-1} in each panel. The narrow absorption at this velocity seen in the spectra of M4 and M5 is an artifact from the sidelobes of M1.

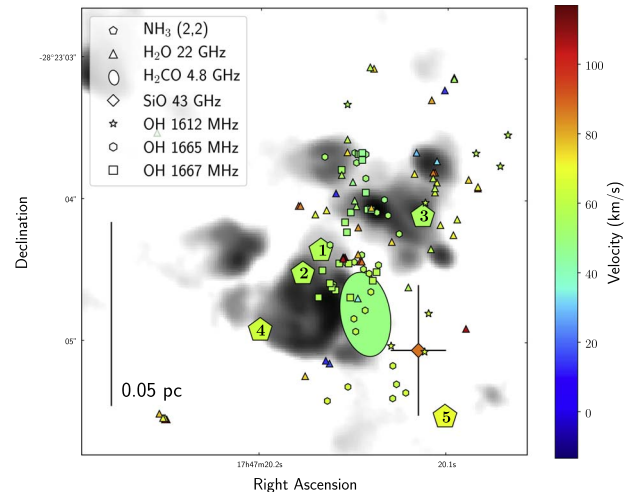


Figure 4. Position of the $^{14}\text{NH}_3$ (2,2) masers detected toward Sgr B2 (M), overlaid on a 3 mm ALMA continuum map (Project 2016.1.00550.S, PI: A. Ginsburg). Also shown are the positions of published maser detections from H_2O (McGrath et al. 2004), OH (Gaume & Claussen 1990), SiO (Morita et al. 1992), and H_2CO (Mehringer et al. 1994). Only the OH masers brighter than 1 Jy are shown, due to the large number detected in this region. The positions of all masers except SiO are determined relative to the continuum emission, and should have positional uncertainty $<0''.5$, smaller than the plotted points. The H_2CO maser emitting region is partially resolved and plotted as an ellipse.

$^{14}\text{NH}_3$ masers, the only observed (1, 1) maser occurs in an outer hyperfine satellite component; Gaume et al. 1996). The maser velocity is also consistent with the velocity of relatively narrow metastable line emission seen in the DnC-configuration

¹³ All listed brightness temperatures are lower limits, as the maser spots are spatially unresolved.

¹⁴ The inner and outer hyperfine satellites in the (2,2) line are offset from the main hyperfine line component by ± 16.6 and $\pm 25.8 \text{ km s}^{-1}$, respectively.

Table 1
Measured Maser Spot Parameters

Source	R.A.	Decl.	v_{cen} (km s^{-1})	v_{fwhm} (km s^{-1})	Peak T_{MB} (K)
M1	17 ^h 47 ^m 20 ^s .167 ± 0.001	−28°23′4″.36 ± 0.01	57.22 ± 0.01	1.64 ± 0.02	90900 ± 1000
M2	17 ^h 47 ^m 20 ^s .177 ± 0.001	−28°23′4″.52 ± 0.02	57.68 ± 0.04	2.13 ± 0.10	21100 ± 800
M3	17 ^h 47 ^m 20 ^s .113 ± 0.002	−28°23′4″.11 ± 0.04	54.99 ± 0.20	3.89 ± 0.47	3900 ± 400
M4	17 ^h 47 ^m 20 ^s .200 ± 0.001	−28°23′4″.92 ± 0.02	64.05 ± 0.51	2.15 ± 1.19	700 ± 300
M5	17 ^h 47 ^m 20 ^s .101 ± 0.001	−28°23′5″.52 ± 0.02	69.21 ± 0.46	3.43 ± 1.09	700 ± 200

observations 4'' to the west. However, the maser velocity is not consistent with the velocity of $^{14}\text{NH}_3$ metastable and nonmetastable line emission observed 3'' to the south, which appears to be closer to 70 km s^{-1} .

Comparing the maser positions to the radio continuum in Figure 4, we do not see a clear correspondence between these masers and radio continuum: only four of the five masers overlap with continuum emission, and these tend to be located on the edge of the H II regions in Sgr B2 (M). Interestingly, M1 is located within 0''.2 of an increase in continuum emission from source ‘‘F3c’’ detected in De Pree et al. (2014). We also compare the position of the (2,2) masers to a number of other masers, both rare and common, that are also seen in Sgr B2 (M). This includes 1612, 1665, and 1667 MHz OH masers (Gaume & Claussen 1990), 22 GHz H_2O masers (McGrath et al. 2004), a 4.8 GHz H_2CO maser (Mehring et al. 1994), and a 43 GHz $J = 1 - 0, v = 1$ SiO maser (Morita et al. 1992). We have used published figures of the masers and the simultaneously observed continuum emission to align the maser positions with our continuum maps. We adjust the positions of the H_2O masers by +0''.16 in R.A. and +0''.54 in decl. to match our reference frame. We also adjust the position of the OH masers by +0''.84 in decl. and the H_2CO maser by +0''.42 in decl.. No corresponding continuum map for the 43 GHz SiO maser is published in Morita et al. (1992), so we adopt their published position and estimates of the absolute positional uncertainty. The position of these other masers relative to the (2,2) masers is shown in Figure 4. None of the other masers observed in Sgr B2 (M) appear to overlap with the (2,2) maser in both position and velocity, though there is a weak ($< 2J_y$) OH 1665 MHz maser within 0''.1 of M1 and offset by $\sim 5 \text{ km s}^{-1}$.

4. Discussion

4.1. Interpreting the (2,2) Maser in Sgr B2 (M)

This is the first $^{14}\text{NH}_3$ (2,2) maser seen in any source. It is a relatively strong maser, with brightness temperatures constrained to be $> 10^4 \text{ K}$ by the A-configuration observations. This is among the brightest $^{14}\text{NH}_3$ masers that have been reported, which typically have limits on their brightness temperatures of $> 10^2 - 10^5 \text{ K}$ (Madden et al. 1986; Wilson et al. 1991; Hofner et al. 1994; Mangum & Wootten 1994; Zhang & Ho 1995; Gaume et al. 1996; Walsh et al. 2007; Hunter et al. 2008; Hoffman & Kim 2011; Hoffman & Joyce 2014; Goddi et al. 2015), with only a single very long baseline interferometry (VLBI) measurement of the $^{14}\text{NH}_3$ (9,6) maser having a brightness temperature $> 10^{13} \text{ K}$ (Pratap et al. 1991).

The most unique characteristic of the observed (2,2) masers is their line width. In the A-configuration observations, line profiles of individual maser spots are well resolved, having widths of up to 4 km s^{-1} . Narrow ($< 1 \text{ km s}^{-1}$) or unresolved widths are typical of most other observed NH_3 masers. As

individual masers show nonthermal line widths, we must assume that multiple masers are present, and that the extreme or unique physical conditions that lead to these masers are relatively common in this region. Given that both the (2,2) masers and the nearby SiO maser show relatively broad line widths over a compact region, an intriguing possibility is that these masers could arise in or near rotating protostellar disks (e.g., as in the SiO masers around Orion’s source I (Goddi et al. 2009; Matthews et al. 2010).

Given limits on the observed maser spot sizes of $\lesssim 1000 \text{ au}$, the observed (2,2) maser line widths could be consistent with Keplerian rotation in the disk of a low- or intermediate-mass protostar. A line width of $2 - 4 \text{ km s}^{-1}$ for a disk with a radius of 400 au would be consistent with rotation around a central mass of $0.5 - 2 M_{\odot}$. In the future, one might be able to test whether the $^{14}\text{NH}_3$ masers arise from such organized or compact circumstellar structures by making VLBI observations of these masers. However, such low-mass protostellar sources would be difficult to detect in millimeter continuum emission as imaging near the bright sources in this region is significantly limited by an achievable dynamic range of ~ 5000 with ALMA (Ginsburg et al. 2018).

4.2. The Excitation of the (2,2) Maser

Our observations suggest that maser emission is possible in essentially any metastable transition of $^{14}\text{NH}_3$: of the inversion transitions up to $J = 9$, only the (4,4) and (8,8) lines have not yet been observed to show maser action, though a weak $^{15}\text{NH}_3$ (4,4) maser has been reported (Schilke et al. 1991). However, at present no universally successful mechanism has been proposed for NH_3 masers. Suggested models for NH_3 maser excitation involve three possible mechanisms: (1) radiative excitation from $10 \mu\text{m}$ continuum emission, (2) collisional excitation, and (3) radiative excitation from a chance line overlap.

Current models of nonmetastable maser emission favor mechanism (1), excitation through the $10 \mu\text{m}$ vibrational transitions pumped by infrared emission (Brown & Cragg 1991). However, these theories tend to predict that multiple, adjacent transitions of NH_3 should maser simultaneously (Wilson & Schilke 1993). While masers have been seen in adjacent nonmetastable transitions (Henkel et al. 2013; Hoffman & Joyce 2014), and metastable transitions of ortho- NH_3 (e.g., 6,6 and 9,9 masers; Goddi et al. 2015), no sources have been observed to show maser emission in multiple para- NH_3 transitions. The only published model of a metastable NH_3 involves the second mechanism, pumping the ortho (3,3) transition via collisions with H_2 (Flower et al. 1990; Mangum & Wootten 1994). However, this model does not predict masers in metastable transitions of para- NH_3 (Schilke et al. 1991), and cannot explain observations of simultaneous maser emission in the ortho- (4,3) and (3,3) lines of $^{15}\text{NH}_3$ (Schilke et al. 1991). Mechanism (3), line overlap, is not currently

avored to explain any of the observed NH_3 masers (e.g., as discussed in Goddi et al. 2015). Indeed, the detection of maser emission in the (2,2) line makes this more unlikely as a general mechanism to explain the metastable para- NH_3 masers, as separate instances of line overlap would be needed to pump each of the (1,1), (2,2), (5,5), and (7,7) lines.

As none of the existing three simple models provide a satisfactory explanation for these masers, we suggest that the excitation of the metastable para- NH_3 masers is likely complicated, and may require a confluence of geometry, velocity structure, and possibly both collisional and radiative excitation (rotational and rovibrational transitions of NH_3 occur at a range of infrared wavelengths from 9 to 400 μm , and the vibrational transitions in particular may be influenced by the shape of the overlapping 9.7 μm silicate absorption feature, as noted by Barentine & Lacy 2012). Devising and validating such a complex model will likely require the availability of collisional coefficients for states above $J = 6$, which is the limit of currently published data (e.g., Bouhafs et al. 2017).

4.3. The (2,2) Maser as a Probe of Star-forming Regions

As $^{14}\text{NH}_3$ is a common probe of gas in star-forming regions, particularly the (1,1) and (2,2) lines, it is somewhat surprising that masers in this line have not previously been seen. Lu et al. (2014) surveyed 62 high-mass star-forming regions in the $^{14}\text{NH}_3$ (1,1) and (2,2) lines with subparsec spatial resolution using the VLA's DnC configuration and did not report any (2,2) maser emission. With an 800 K brightness temperature for this maser in our DnC-configuration observations, similar masers in other star-forming regions should have been readily apparent. It appears likely then that, like other metastable $^{14}\text{NH}_3$ masers, this maser is quite rare, which would limit its general usefulness as a star formation probe.

The (2,2) maser is the first NH_3 maser confirmed to exist in Sgr B2. This increases the number of star-forming regions known to host either metastable or nonmetastable NH_3 masers from seven to eight. We suggest that more massive star-forming regions should be carefully surveyed for NH_3 masers in a wide variety of nonmetastable and metastable transitions, in order to better understand their overall incidence and association with various stages and structures of star formation, and to provide improved constraints for models of NH_3 maser excitation.

5. Summary










We report the discovery of the first $^{14}\text{NH}_3$ (2,2) maser, which is detected in the Sgr B2 Main star-forming region. Below, we summarize our main findings.

1. At the high resolution of our VLA A-configuration observations ($0''.1$ or ~ 1000 au) the (2,2) maser breaks into five independent spots with T_B from 700 to 9×10^4 K. These $^{14}\text{NH}_3$ masers are not spatially or kinematically coincident with any other masers in this region, or with the peaks of the observed radio continuum emission.
2. The $^{14}\text{NH}_3$ (2,2) masers are spatially unresolved in the A-configuration observations, but have unusually broad line widths of 1.5–4 km s^{-1} , which could trace the kinematics of circumstellar gas.
3. The (2,2) maser is the only $^{14}\text{NH}_3$ maser seen in this region and the fourth metastable transition of para- $^{14}\text{NH}_3$ observed

to be a maser, which increases the inconsistencies between the observed NH_3 masers and the existing models for this emission.

This material is based upon work supported by the National Science Foundation under grant Nos. AST-1813765 and AST-1615311. P.S. and A.S.M. acknowledge support from the Deutsche Forschungsgemeinschaft (DFG) via the Sonderforschungsbereich SFB 956 (project A6).

ORCID iDs

E. A. C. Mills  <https://orcid.org/0000-0001-8782-1992>
 A. Ginsburg  <https://orcid.org/0000-0001-6431-9633>
 A. R. Clements  <https://orcid.org/0000-0001-8209-2989>
 P. Schilke  <https://orcid.org/0000-0003-2141-5689>
 Á. Sánchez-Monge  <https://orcid.org/0000-0002-3078-9482>
 K. M. Menten  <https://orcid.org/0000-0001-6459-0669>
 N. Butterfield  <https://orcid.org/0000-0002-4013-6469>
 A. Schmiedeke  <https://orcid.org/0000-0002-1730-8832>
 C. G. De Pree  <https://orcid.org/0000-0003-3115-9359>

References

- Barentine, J. C., & Lacy, J. H. 2012, *ApJ*, 757, 111
 Bouhafs, N., Rist, C., Daniel, F., et al. 2017, *MNRAS*, 470, 2204
 Brown, R. D., & Cragg, D. M. 1991, *ApJ*, 378, 445
 Corby, J. F., Jones, P. A., Cunningham, M. R., et al. 2015, *MNRAS*, 452, 3969
 De Pree, C. G., Goss, W. M., & Gaume, R. A. 1998, *ApJ*, 500, 847
 De Pree, C. G., Peters, T., Mac Low, M.-M., et al. 2014, *ApJL*, 781, L36
 Faure, A., Remijan, A. J., Szalewicz, K., & Wiesenfeld, L. 2014, *ApJ*, 783, 72
 Flower, D. R., Offer, A., & Schilke, P. 1990, *MNRAS*, 244, 4P
 Gaume, R. A., & Claussen, M. J. 1990, *ApJ*, 351, 538
 Gaume, R. A., Johnston, K. J., Nguyen, H. A., et al. 1991, *ApJ*, 376, 608
 Gaume, R. A., Wilson, T. L., & Johnston, K. J. 1996, *ApJL*, 457, L47
 Ginsburg, A., Bally, J., Barnes, A., et al. 2018, *ApJ*, 853, 171
 Goddi, C., Greenhill, L. J., Chandler, C. J., et al. 2009, *ApJ*, 698, 1165
 Goddi, C., Henkel, C., Zhang, Q., Zapata, L., & Wilson, T. L. 2015, *A&A*, 573, A109
 Gravity Collaboration, Abuter, R., Amorim, A., et al. 2018, *A&A*, 615, L15
 Henkel, C., Wilson, T. L., Asiri, H., & Mauersberger, R. 2013, *A&A*, 549, A90
 Hoffman, I. M., & Joyce, S. A. 2014, *ApJ*, 782, 83
 Hoffman, I. M., & Kim, S. S. 2011, *ApJL*, 739, L15
 Hofner, P., Kurtz, S., Churchwell, E., Walmsley, C. M., & Cesaroni, R. 1994, *ApJL*, 429, L85
 Hunter, T. R., Brogan, C. L., Indebetouw, R., & Cyganowski, C. J. 2008, *ApJ*, 680, 1271
 Johnston, K. J., Stolovy, S. R., Wilson, T. L., Henkel, C., & Mauersberger, R. 1989, *ApJL*, 343, L41
 Kraemer, K. E., & Jackson, J. M. 1995, *ApJL*, 439, L9
 Lu, X., Zhang, Q., Liu, H. B., Wang, J., & Gu, Q. 2014, *ApJ*, 790, 84
 Madden, S. C., Irvine, W. M., Matthews, H. E., Brown, R. D., & Godfrey, P. D. 1986, *ApJL*, 300, L79
 Mangum, J. G., & Wootten, A. 1994, *ApJL*, 428, L33
 Martín-Pintado, J., Gaume, R. A., Rodríguez-Fernández, N., de Vicente, P., & Wilson, T. L. 1999, *ApJ*, 519, 667
 Matthews, L. D., Greenhill, L. J., Goddi, C., et al. 2010, *ApJ*, 708, 80
 Mauersberger, R., Henkel, C., & Wilson, T. L. 1987, *A&A*, 173, 352
 Mauersberger, R., Wilson, T. L., & Henkel, C. 1986, *A&A*, 160, L13
 McGrath, E. J., Goss, W. M., & De Pree, C. G. 2004, *ApJS*, 155, 577
 Mehringer, D. M., Goss, W. M., & Palmer, P. 1994, *ApJ*, 434, 237
 Mills, E. A. C., Butterfield, N., Ludovici, D. A., et al. 2015, *ApJ*, 805, 72
 Morita, K.-I., Hasegawa, T., Ukita, N., Okumura, S. K., & Ishiguro, M. 1992, *PASJ*, 44, 373
 Ott, J., Weiss, A., Henkel, C., & Walter, F. 2005, *ApJ*, 629, 767
 Pratap, P., Menten, K. M., Reid, M. J., Moran, J. M., & Walmsley, C. M. 1991, *ApJL*, 373, L13

- Qin, S.-L., Schilke, P., Rolffs, R., et al. 2011, [A&A](#), **530**, L9
- Qin, S.-L., Zhao, J.-H., Moran, J. M., et al. 2008, [ApJ](#), **677**, 353
- Reid, M. J., Menten, K. M., Zheng, X. W., Brunthaler, A., & Xu, Y. 2009, [ApJ](#), **705**, 1548
- Sánchez-Monge, Á, Schilke, P., Schmiedeke, A., et al. 2017, [A&A](#), **604**, A6
- Schilke, P., Walmsley, C. M., & Mauersberger, R. 1991, [A&A](#), **247**, 516
- Scoville, N. Z., Solomon, P. M., & Penzias, A. A. 1975, [ApJ](#), **201**, 352
- van der Walt, S., Schonberger, J. L., Nunez-Iglesias, J., et al. 2014, [PeerJ](#), **2**, e453
- Vogel, S. N., Genzel, R., & Palmer, P. 1987, [ApJ](#), **316**, 243
- Walsh, A. J., Longmore, S. N., Thorwirth, S., Urquhart, J. S., & Purcell, C. R. 2007, [MNRAS](#), **382**, L35
- Wilson, T. L., Gaume, R., & Johnston, K. J. 1991, [A&A](#), **251**, L7
- Wilson, T. L., & Henkel, C. 1988, [A&A](#), **206**, L26
- Wilson, T. L., Henkel, C., & Hüttemeister, S. 2006, [A&A](#), **460**, 533
- Wilson, T. L., Henkel, C., & Johnston, K. J. 1990, [A&A](#), **229**, L1
- Wilson, T. L., & Schilke, P. 1993, in *Lecture Notes in Physics*, Vol. 413, *Astrophysical Masers*, ed. A. W. Clegg & G. E. Nedoluha (Berlin: Springer), 123
- Zhang, Q., & Ho, P. T. P. 1995, [ApJL](#), **450**, L63